Materials Transactions, Vol. 43, No. 4 (2002) pp. 667 to 673

Synthesis of Fe–Cu Nanoparticles by Mechanochemical Processing Using a Ball Mill *1

Yoshikazu Todaka[1, *2], Paul Gerard McCormick[2], Koichi Tsuchiya[1] and Minoru Umemoto[1]

[1]*Department of Production Systems Engineering, Toyohashi University of Technology, Toyohashi 441-8580, Japan*
[2]*Department of Mechanical and Materials Engineering, University of Western Australia, Nedlands, WA 6907, Australia*

Fe–Cu nanoparticles were synthesized by mechanochemical processing, which utilizes the reaction of $FeCl_3$ and $CuCl_2$ with Na during ball milling. Morphologies, structures and magnetic properties of the synthesized nanoparticles were investigated. The crystallite size and mean particle size of the washed nanoparticles after 84 h milling were approximately 9 nm and 50 nm, respectively. During ball milling, the crystallite size remained constant at approximately 14 nm, while the particle size increased. The elemental mapping images of Fe and Cu by imaging filter revealed that the synthesized nanoparticles were a solid solution of the Fe–Cu system. It was seen that numerous hexagonal plates of $Fe(OH)_2$ exist in the washed nanoparticles. The plates had a few nm in thickness and a few hundreds nm in diameter. The coercivity of the synthesized Fe–Cu nanoparticles after 48 h milling was as high as 33.5 kA/m. This is because the particle is close to the critical size for a single magnetic domain of α-Fe.

(Received November 22, 2001; Accepted February 6, 2002)

Keywords: *iron-copper solid solution, non-equilibrium phase, nanoparticle, mechanochemical reaction, ball mill, microstructure, magnetic property*

1. Introduction

Mechanochemical processing makes use of enhancement of chemical reactions by mechanical energy. Ding and co-workers[1–8] have synthesized a number of metallic and oxide nanoparticles, such as Fe, Cu, Co, Ni, Fe_2O_3, Cr_2O_3 and Al_2O_3, by mechanochemical processing using a ball mill. In the present study, this method has been applied to synthesize nanoparticles of non-equilibrium Fe–Cu solid solution by the simultaneous progress of the following two reactions:

$$FeCl_3 + 3Na \rightarrow Fe + 3NaCl \quad (1)$$

$$CuCl_2 + 2Na \rightarrow Cu + 2NaCl \quad (2)$$

The Fe–Cu binary system possesses a large positive enthalpy of mixing and thus is virtually immiscible in the whole range of composition in equilibrium. A solid solution of the Fe–Cu system can be obtained only by non-equilibrium techniques, such as mechanical alloying[9,10] or vapor deposition.[11] The reactions (1) and (2) result in the formation of Fe–Cu nanoparticles embedded in the matrix of by-product NaCl. Provided that the volume fraction of NaCl is sufficiently large, the metal nanoparticles separately nucleate and grow in the NaCl matrix. In this study, the volume fraction of NaCl in the product mixture is calculated to be 95.8 vol%. Subsequent removal of the NaCl results in the powder consisting of nanometer sized particles. NaCl powder also has another important role to suppress combustive reaction during the milling. In the previous investigations,[1–4] Fe and Cu nanoparticles were synthesized through the reactions (1) and (2), respectively, and these reactions proceed with unstable self-propagating combustion due to the large enthalpy changes in the reactions ($\Delta H_{293\,K} = -834$ kJ for (1), $\Delta H_{293\,K} = -604$ kJ for (2)).[12] The combustive reaction is undesirable for the synthesis of nanoparticles since it causes a significant temperature rise, leading to a larger particle size. Therefore, the suppression of the combustive reaction is important for the synthesis of uniform sized nanoparticles in this process. The previous studies suggested that the combustion reaction could be initiated by ball/powder collision events during milling.[1–5,13,14] Reduction of collision energy and dilution of reactants are considered as the possible means for avoiding combustive reaction. In this study, the combustive reaction was suppressed by adding NaCl powder into the starting mixture, to decrease the collision frequency between the reactants.

This paper describes the results of a study on the evolution of nanostructures and magnetic properties during the mechanochemical processing of $FeCl_3$ and $CuCl_2$ with Na to form Fe–Cu nanoparticles. It was also found that the formation of thin hexagonal plates of $Fe(OH)_2$ accompanies the Fe–Cu nanoparticles formation.

2. Experimental Procedure

2.1 Synthesis of nanoparticles

The starting materials used in this study were anhydrous $FeCl_3$ (> 98%), $CuCl_2 \cdot H_2O$ (> 99%) powders and Na blocks (< 5 mm). NaCl (> 99.5%) powder was added as a diluent to the starting mixture in order to avoid combustive reaction. The chloride powders were dried prior to milling. The starting mixture (5 g), that consists of $FeCl_3 + CuCl_2 + 5Na + 7NaCl$, was loaded and sealed together with ϕ4.8 mm steel balls (15 g) in a hardened steel vial under Ar atmosphere. The reactants were milled using a SPEX 8000 mixer/mill for various times (up to 84 h). The vial temperature was kept constant by air-cooling. The outside temperature of the vial was mon-

*1 This Paper was Presented at the Autumn Meeting of the Japan Institute of Metals, held in Kanazawa, on November 20, 1999.
*2 Graduate Student, Toyohashi University of Technology.

itored during the course of milling using a Chromel-Alumel thermocouple attached to its surface. An abrupt increase of the vial temperature indicates that the combustive reaction occurred. In this study, all the milling processes were carried out without the combustive reaction. The Fe–Cu nanoparticles were separated from NaCl through a following washing process. The as-milled powders were dispersed ultrasonically in the deionized and deoxygenated water. Then, the Fe–Cu particles and NaCl solution were separated using a magnet or a centrifuge. After washing, the Fe–Cu particles were dried under vacuum at room temperature and directly transferred to a glove box filled with Ar.

2.2 Characterization of nanoparticles

Structure analysis of the washed powders was carried out on a Siemens 5000 X-ray diffractometer with Ni-filtered Cu–K_α radiation generated at 40 kV/35 mA. A sealed and Ar filled sample holder was used to prevent oxidation of the sample.

Compositions of the washed powders were analyzed on a JEOL JSM-6300 scanning electron microscope (SEM) equipped with an energy dispersive X-ray spectroscope (EDX). The analysis was carried out on a sampling area of 200 µm × 160 µm. Morphologies of the washed powders were observed on a JEOL 6300F field emission SEM (FESEM). Both SEM and FESEM investigations were performed at an acceleration voltage of 20 kV.

Morphologies, nanostructures and compositions of the washed powders were investigated on an analytical transmission electron microscopy (TEM) using a Philips 430 equipped with a Gatan Imaging Filter GIF200 incorporated in an electron energy loss spectroscope (EELS) for elemental mapping at an acceleration voltage of 300 kV. A sample holder in which sample could be sealed was used, so that the sample was set up in the TEM without exposure to air. The synthesized nanoparticles were put onto a carbon film supported on a copper grid directly from the washed powder, and then the grid was loaded to the sample stage in the glove box. These investigations were also done on a high-resolution TEM (HRTEM) using a JEOL JEM-2010 equipped with a NORAN Voyager III EDX at an acceleration voltage of 200 kV. Nanobeam diffraction (NBD) mode on the JEM-2010 was used to obtain electron diffraction patterns from individual nanoparticles. The synthesized nanoparticles were dispersed ultrasonically in iso-propyl alcohol, and a few drops of the mixture were then pipetted onto a Ni grid just before insertion into the JEM-2010 TEM, thus minimizing the possibility of oxidation in air.

Specific surface areas of the washed powders were measured with the five-points BET (Brunauer-Emmett-Teller) method using a Micromeritics Gemini 2360. Mean diameters of particles were estimated from the specific surface area.

Magnetic measurements of the as-milled powders were carried out on an Oxford 3001 vibrating sample magnetometer (VSM) with a maximum applied field of 2.4 MA/m at room

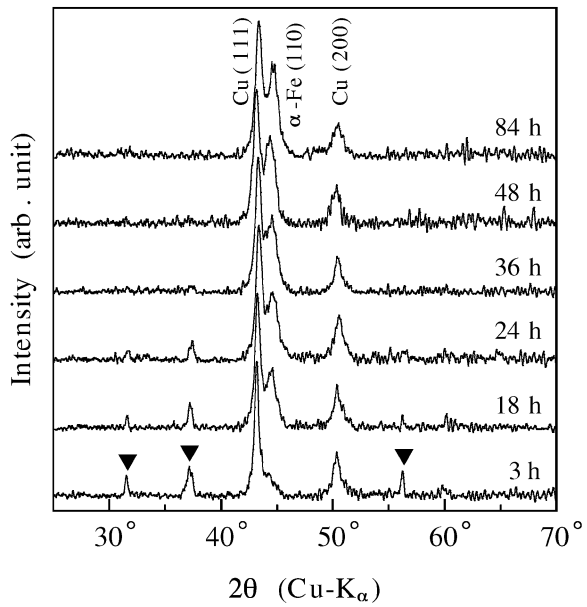

Fig. 2 XRD patterns of the washed powders for various milling times. The triangles denote the peaks are from the hexagonal plates (see text).

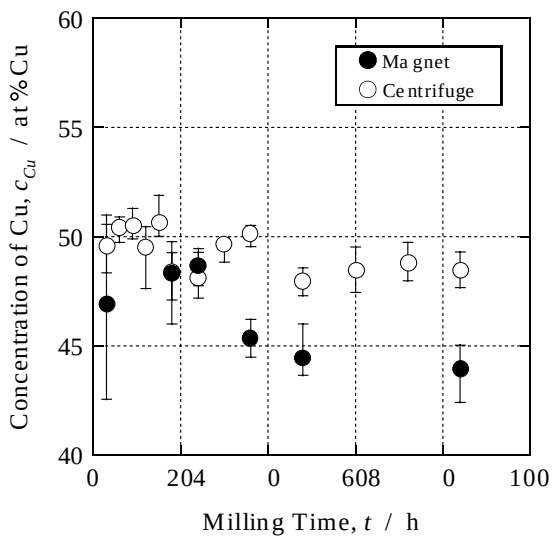

Fig. 1 Compositions of the washed powders for various milling times. The error bars indicate the maximum and minimum values of 5 sampling points.

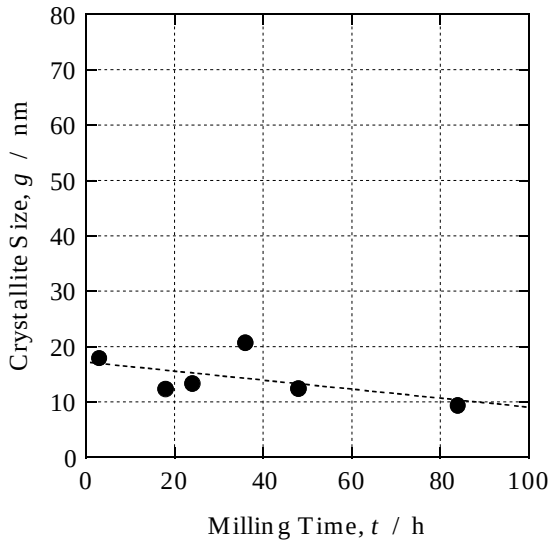

Fig. 3 Crystallite sizes of the washed nanoparticles for various milling times, which estimated from the width of the Cu (200) peak in the XRD patterns (Fig. 2).

temperature. The as-milled powders were cold-pressed to the shape of cylinder (ϕ5 mm × t3.5 mm) in a glove box. The pressed samples were sealed and fixed in a polymer vial using wax. Magnetization at the maximum field of 2.4 MA/m was taken to be the saturation magnetization.

3. Results and Discussion

Figure 1 reveals the compositions of the washed powders for various milling times, analyzed using the EDX in the SEM. The average composition of the powders collected by using a magnet was approximately Fe–46.3 at%Cu, slightly deficient in Cu than the nominal composition (Fe–50.0 at%Cu). On the other hand, the average composition of the powders collected by a centrifuge was approximately Fe–49.3 at%Cu, closer to the nominal composition. It is due to that the synthesized Cu-rich particles could not be collected completely by using a magnet, because Fe clusters in the fcc-

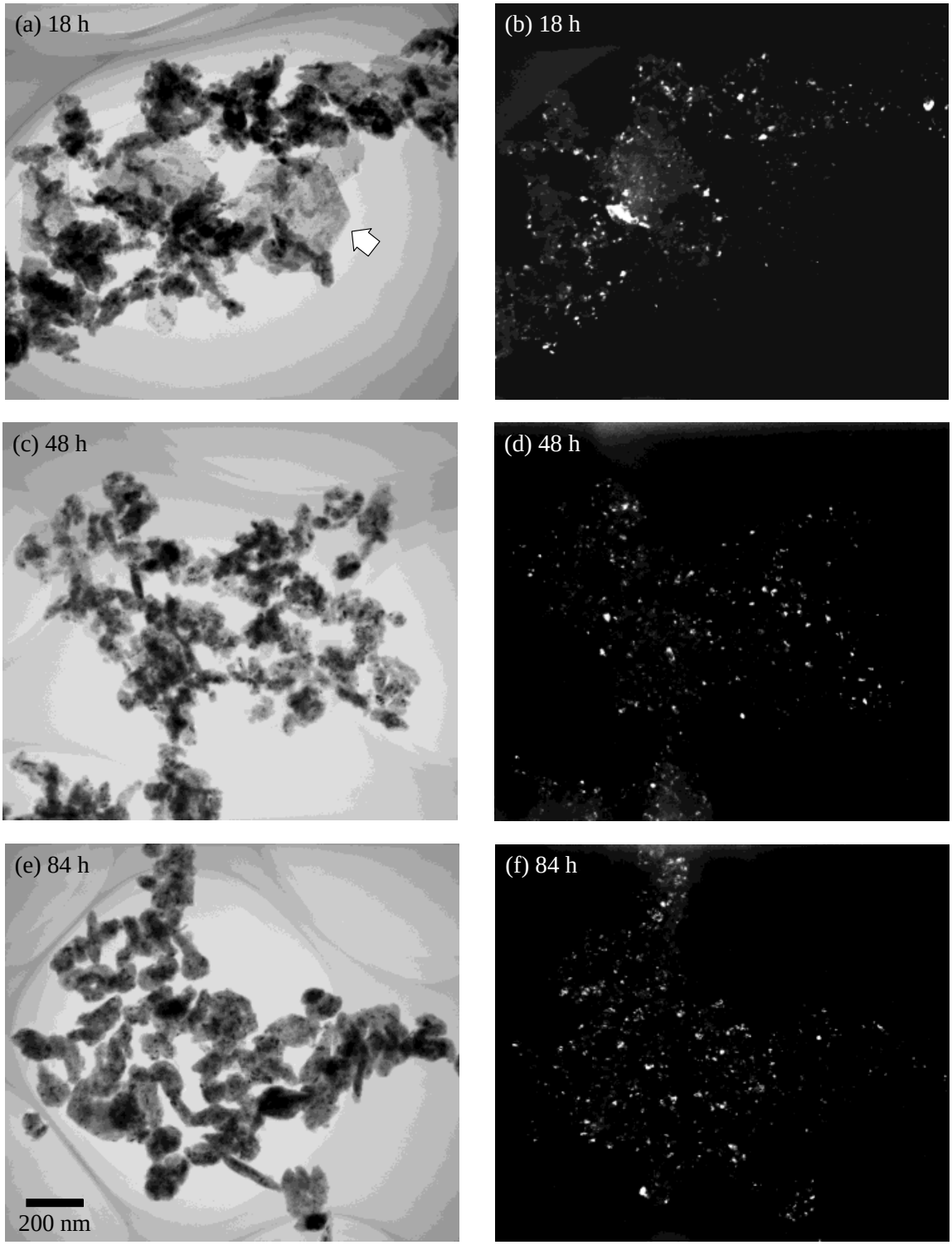

Fig. 4 TEM BF images ((a), (c) and (e)) and DF images ((b), (d) and (f)) of the washed powders for various milling times. The arrow denotes the hexagonal plate.

Cu matrix behave as γ-Fe,[11,15] in which the magnetic moment of Fe atoms is extremely small. The powders collected using a centrifuge, however, were exposed to air in the course of collecting, leading to the oxidation of the Fe–Cu nanoparticles.

Figure 2 reveals the X-ray diffraction (XRD) patterns of the washed powders for various milling times. The peaks corresponding to bcc and fcc phases could be identified provided that the lattice parameters of bcc and fcc phases were close to those of α-Fe and Cu, respectively. It can be seen that Fe and Cu particles are obtained after removing the remaining reactants and NaCl by the appropriate washing process. In the XRD patterns, the peaks other than those of Fe and Cu, denoted by the triangles in Fig. 2, are found for the powders milled for shorter time (< 24 h). Those peak positions were close to those of $Fe(OH)_2$ (hexagonal, $a = 0.32800$ nm, $c = 0.460500$ nm).[16]

The crystallite sizes of the washed Fe–Cu nanoparticles were estimated using the Scherrer equation from the width of the Cu (200) peak in the XRD patterns.[17] Figure 3 reveals the crystallite sizes of the washed nanoparticles for various milling times. The correction of the machine error was carried out with the Warren's method,[17] using Cu powder with the purity of 99.999% and the particle size of 150 μm as the standard sample. The crystallite size of Cu was approximately 14 nm, and remained constant with milling time. The crystalline size was also estimated by TEM observations.

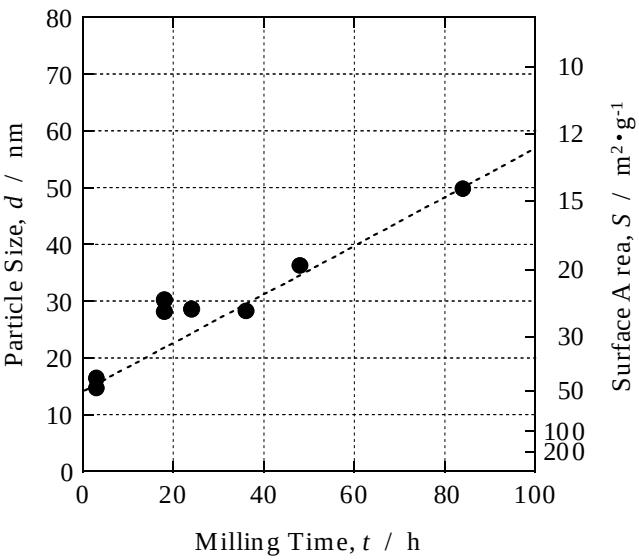

Fig. 5 Particle sizes of the washed powders for various milling times.

Figure 4 shows the TEM images (bright field (BF), (a), (c) and (e), and dark field (DF), (b), (d) and (f)) of the washed Fe–Cu nanoparticles after 18 h, 48 h and 84 h milling. In the DF images, the strongly reflecting regions corresponded to the rings of α-Fe (110) or Cu (111). The DF images show that there is no remarkable difference in the crystalline size of Fe and Cu, and therefore it is suggested that both sizes are approximately 14 nm with the Cu crystallite size estimated from the XRD peak widths. The crystalline size remained constant with milling time, which was in good agreement with the crystallite size (Fig. 3).

Figure 5 reveals the mean particle sizes estimated from the specific surface areas of the washed powders for various milling times. The particle size increased with milling time, to be approximately 16 nm and 50 nm for powders milled for 3 h and 84 h, respectively. These results were also in good agreement with those estimated from the TEM BF images shown in Fig. 4. Nevertheless, the particle size remains in the order of ten nanometers. It is inferred from these results that the by-product of NaCl successfully suppressed the welding between particles during milling.

In the washed powder for 18 h milling shown in Fig. 4(a), two kinds of morphologies were observed, an irregular and a hexagonal shape denoted by the arrow. The FESEM images also show such morphologies in Fig. 6. The washed powder for 18 h milling included the numerous hexagonal plates in comparison with the powder for 48 h milling. The plates are generally with a thickness of a few nanometers and a diameter of approximately 300 nm in the powder milled for 18 h. Although the mean particle size increased linearly with milling time (Fig. 5), the size deviation reached a maximum around 18 h milling. It is attributed to that the washed powder milled for around 18 h included the numerous hexagonal plates.

Figure 7 shows the TEM BF, and elemental mapping im-

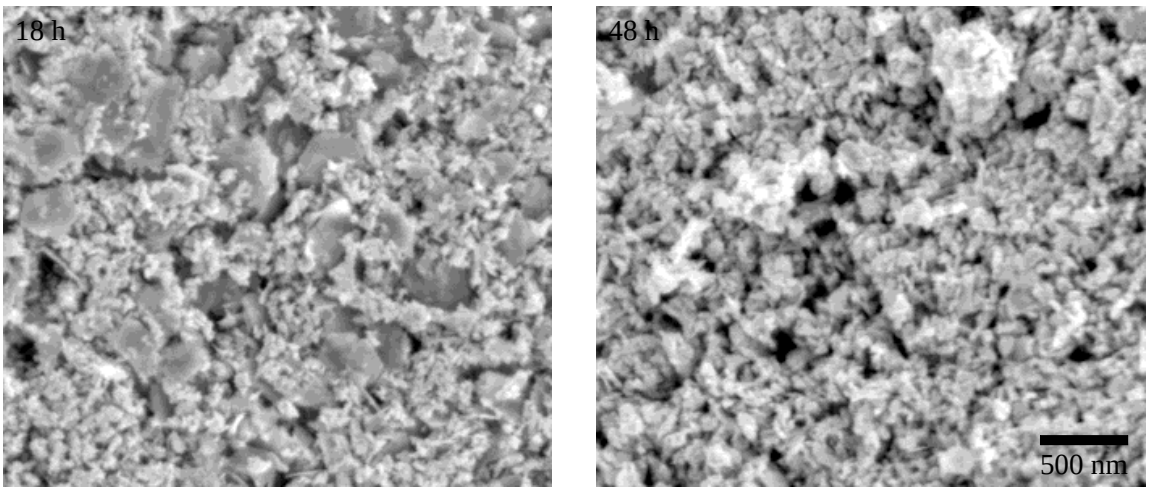

Fig. 6 FESEM images of the washed powders after 18 h and 48 h milling.

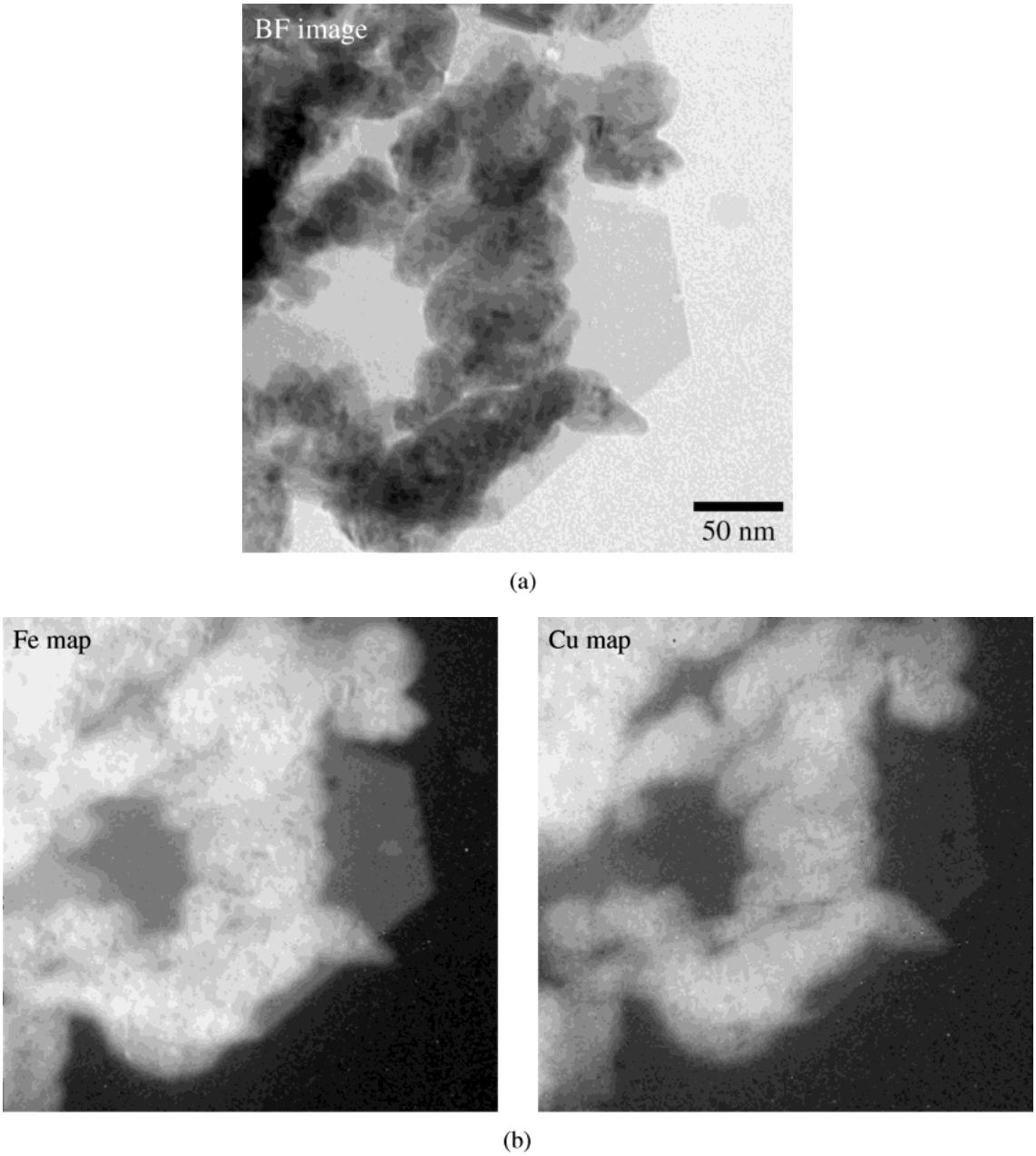

Fig. 7 TEM BF (a) and elemental mapping (b) images of the washed powder after 48 h milling.

ages of Fe and Cu using the imaging filter for the washed powder after 48 h milling. In the mapping images, the signal from both Fe and Cu can be seen in the whole area of the particles, suggesting that the nanoparticles are a solid solution of the Fe–Cu system. The mapping images also exhibit mottled contrasts due to the non-uniformity in the composition. The size of the contrast is smaller than the crystallite size (about 14 nm) determined by XRD pattern and the grain size determined by TEM DF image. Also the mapping images show that the hexagonal plate does not contain Cu atoms because the signal from Cu can hardly be seen.

The structure and composition of the hexagonal plate in the washed powder milled for 18 h were investigated using the HRTEM with the EDX, as are shown in Fig. 8. The NBD pattern and the EDX spectrum from the area enclosed with a circle in the TEM BF image (Fig. 8(a)) are shown in Figs. 8(b) and (c), respectively. The NBD pattern suggests that the hexagonal plates are α-Fe_2O_3 with [001] normal, and the EDX spectrum exhibited only Fe peaks (Ni peaks were confirmed to be from a Ni grid). Figure 9 also shows the HRTEM image and the NBD pattern of the hexagonal plate in the washed powder milled for 84 h. The lattice space was 0.24 nm, which was close to the reference value of α-Fe_2O_3 {200} plane (0.25178 nm[18)]). It is therefore suggested that the hexagonal plates are α-Fe_2O_3 with [001] normal. However, the XRD patterns (Fig. 2) indicated that the hexagonal plates are $Fe(OH)_2$. These results suggested that $Fe(OH)_2$ was transformed into α-Fe_2O_3 by iso-propyl alcohol that was used to disperse the synthesized nanoparticles in the TEM observations. The mechanism for the formation of the hexagonal plates has not been clarified yet. In the previous study of Fe nanoparticles synthesis with the reaction (1), however, these

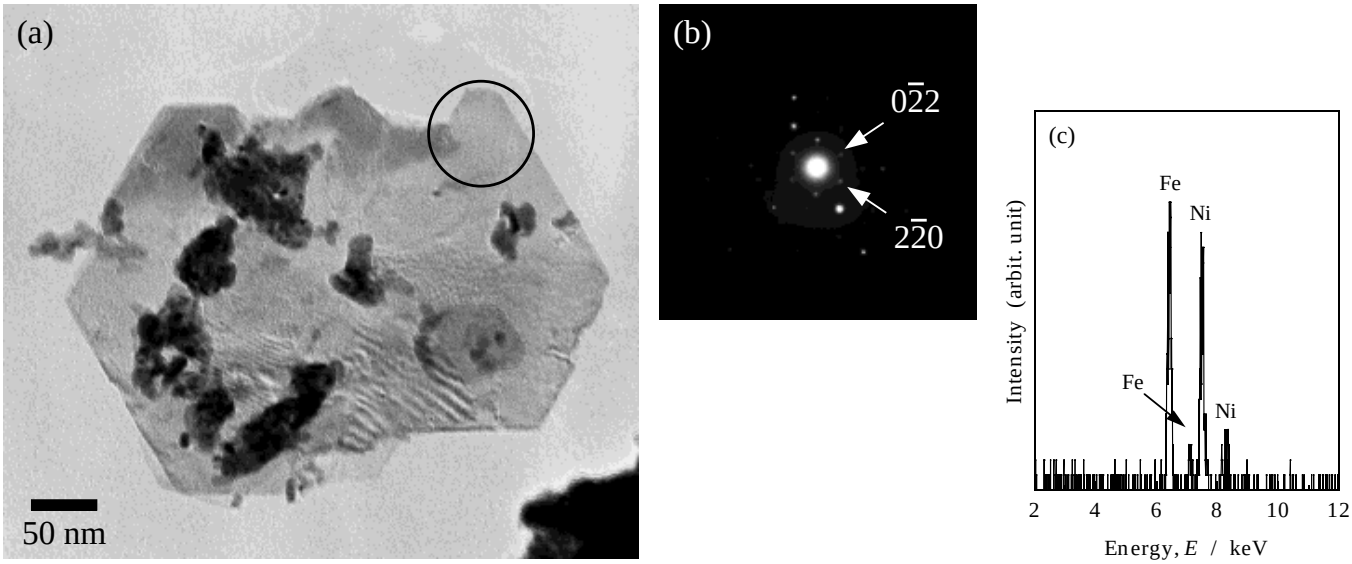

Fig. 8 TEM BF image (a), NBD pattern (b) and EDX spectrum (c) of the hexagonal plate in the washed powder after 18 h milling.

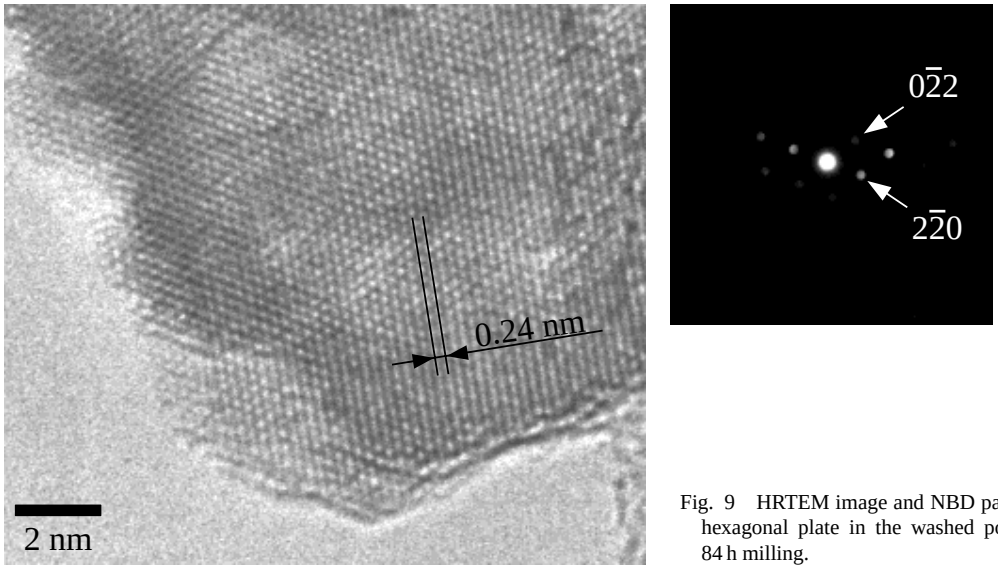

Fig. 9 HRTEM image and NBD pattern of the hexagonal plate in the washed powder after 84 h milling.

hexagonal plates were not found,[1–3] suggesting that the existence of Cu catalyzed the formation of the plates. Also, $Fe(OH)_2$ plates seem to form in the course of washing because $Fe(OH)_2$ contains two hydroxyl radicals. The plates may be synthesized as a result of the reaction of water and iron ions in the colloid consisting of the remaining reactants and Fe–Cu nanoparticles.

Figure 10 reveals the saturation magnetization (M_S) and coercivity (H_C) values of the as-milled powders for various milling times. The M_S values increase rapidly with milling time in the first 18 h milling, and levels off upon further (> 18 h). The maximum M_S value was approximately 15.9 μWb·m/kg, which was smaller than the calculated M_S of 18.3 μWb·m/kg for the mixture Fe+Cu+12NaCl. It is because the Fe clusters in the fcc-Cu matrix behave as γ-Fe phase,[11,15] in which the magnetic moment of Fe atoms is extremely small. The progress of the reaction (1) during milling was inferred to nearly complete after 18 h milling from the change of the M_S value, for the reason that the bcc-Fe phase is ferromagnetic with a M_S of 270 μWb·m/kg at room temperature while the magnetizations of $FeCl_3$, $CuCl_2$, Na and Cu are negligibly small. In addition, the result of the composition analysis (Fig. 1) indicated that the reactions (1) and (2) progressed simultaneously, because the compositions of the synthesized Fe–Cu nanoparticles for various milling times were always close to the nominal composition (Fe–50.0 at%Cu). The H_C value increased with milling time in the first 48 h milling, then further milling caused the decrease of the H_C values. The maximum H_C value was approximately 33.5 kA/m. This value is much higher than that of the bulk α-Fe (about 0.1 kA/m). It is attributed to that the particle size is close to the critical size for a single magnetic domain particle of Fe, which is 20–40 nm.[19,20]

4. Conclusion

Fe–Cu nanoparticles synthesized by a mechanochemical processing using a ball mill and a subsequent washing pro-

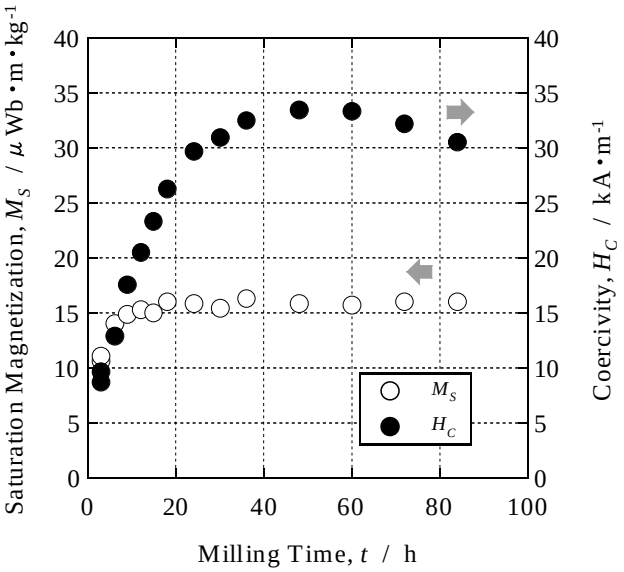

Fig. 10 Saturation magnetization, M_S, and coercivity, H_C, values of the as-milled powders for various milling times.

cess were found to be a solid solution of the Fe–Cu system. The particle size was uniform and approximately 50 nm after 84 h milling. The crystallite size remained constant as approximately 14 nm with milling time. Numerous thin hexagonal plates of $Fe(OH)_2$ are also synthesized. The coercivity of approximately 33.5 kA/m after 48 h milling was found to be much higher than that of the bulk Fe. This can be attributed to the nanometer size of the particles.

REFERENCES

1) J. Ding, W. F. Miao, T. Tsuzuki, P. G. McCormick and R. Street: *Synthesis and Processing of Nanocrystalline Powder*, ed. by D. L. Bouvell (TMS, 1996) pp. 69–79.
2) J. Ding, W. F. Miao, P. G. McCormick and R. Street: Appl. Phys. Lett. **67** (1995) 3804–3806.
3) J. Ding, T. Tsuzuki, P. G. McCormick and R. Street: J. Magn. Magn. Mater. **162** (1996) 271–276.
4) J. Ding, T. Tsuzuki, P. G. McCormick and R. Street: J. Alloys Comp. **234** (1996) L1-L3.
5) J. Ding, T. Tsuzuki, P. G. McCormick and R. Street: J. Phys. D **29** (1996) 2365–2369.
6) J. Ding, T. Tsuzuki and P. G. McCormick: Nano Structured Materials **8** (1997) 739–747.
7) T. Tsuzuki and P. G. McCormick: Acta Mater. **48** (2000) 2795–2801.
8) J. Ding, T. Tsuzuki and P. G. McCormick: J. Am. Ceram. Soc. **79** (1996) 2956–2958.
9) J. Eckert, J. C. Holzer, C. E. Krill III and W. L. Johnson: J. Appl. Phys. **73** (1993) 2794–2802.
10) L. B. Hong and B. Fultz: Acta Mater. **46** (1998) 2937–2946.
11) K. Sumiyama, T. Yoshitake and Y. Nakamura: J. Phys. Soc. Jpn. **53** (1984) 3160–3165.
12) I. Brain: *Thermochemical Data of Pure Substance* (Weinheim, Germany: VCH, 1995).
13) G. B. Schaffer and P. G. McCormick: Metall. Trans. A **23** (1992) 1285–1290.
14) H. Yang and P. G. McCormick: J. Mater. Sci. Lett. **12** (1993) 1088–1091.
15) Y. Ueda, S. Ikeda, Y. Mori and H. Zaman: Mater. Sci. Eng. A **217/218** (1996) 371–375.
16) JCPDS card, 13–0089.
17) B. D. Cullity: *Elements of X-ray diffraction*, (Addison-Wesley, 1978).
18) JCPDS card, 33–0664.
19) W. Gong, H. Li, Z. Zhao and J. Chen: J. Appl. Phys. **69** (1991) 5119–5121.
20) N. Hiratsuka, H. Tomimori, T. Minakawa and K. Kakizaki: J. Jpn Soc. Powder Metall. **43** (1996) 1411–1414.